Improved tribological properties, thermal and colloidal stability of poly-α-olefins based lubricants with hydrophobic MoS2 submicron additives

M.Z. Saidi, A. Pasc, C. El Moujahid, N. Canilho, M. Badawi, C. Delgado-Sánchez, A. Celzard, V. Fierro, R. Peignier, R. Kouitat-Njiwa, et al.

Improved tribological properties, thermal and colloidal stability of poly-α-olefins based lubricants with hydrophobic MoS_2 submicron additives

M. Z. Saidi,[1] A. Pasc,[2*] C. El Moujahid,[1] N. Canilho,[2] M. Badawi,[3] C. Delgado-Sanchez, [4] A. Celzard,[4] V. Fierro,[4] R. Peignier,[5] R. Kouitat-Njiwa,[5] H. Akram,[1*] and T. Chafik[1]

[1] Laboratoire de Génie Chimique et Valorisation des Ressources, Faculté des Sciences et Techniques de Tanger, Université Abdelmalek Essâadi, BP 416, Tanger, Maroc.

[2] L2CM UMR CNRS 7053, Université de Lorraine, 54506, Vandoeuvre-lès-Nancy, France

[3] LPCT UMR CNRS 7019, Université de Lorraine, 54506, Vandoeuvre-lès-Nancy, France

[4] IJL UMR 7198 CNRS, Université de Lorraine, 88000 Epinal, France

[5] IJL UMR 7198 CNRS, Université de Lorraine, 54000 Nancy, France

Corresponding author: andreea.pasc@univ-lorraine.fr, akramhanane@yahoo.fr

Abstract

Hypothesis

Newtonian liquids, usually used as base oil lubricants, exhibit low viscosity under extreme thermal conditions, needed for the functioning of wind turbines. This is directly affecting the colloidal stability and the tribological properties of the formulations containing additives, such as MoS_2. Here, it was hypothesized that the surface hydrophobization of MoS_2 particles will allow for an increased colloidal stability of the resulting formulations, for temperatures as high as 80°C.

Experiments

The antifriction properties and the thermal stability of the designed formulations were determined on submicron MoS_2 particles dispersed in poly-α-olefins (PAO) base oils of different dynamic viscosities (from 32 to 1650 mPa·s at 25°C). The submicron particles of MoS_2 (300-500 nm in diameter) were synthesised by a simple one-pot solvothermal method under mild conditions. The resulting particles were hydrophobized in situ in PAO base oils using alkyltrichlorosilane grafting agents with two chain lengths (C8 and C18).

Findings

The covalent grafting of alkylsilanes through Mo-O-Si bonds was confirmed by DFT calculations and FT-IR measurements. Turbiscan optical analysis revealed that thermal and colloidal stabilities can be significantly improved depending on oil viscosity and chain length of the grafting agent. The formulations in the PAO65 oil remained highly stable (TSI<1), even at 80°C. Herein, we demonstrate the impact of hydrophobization degree on the tribological properties of the lubricants, which, importantly, could reach ultra-low friction coefficients, less than 0.02.

Graphical abstract

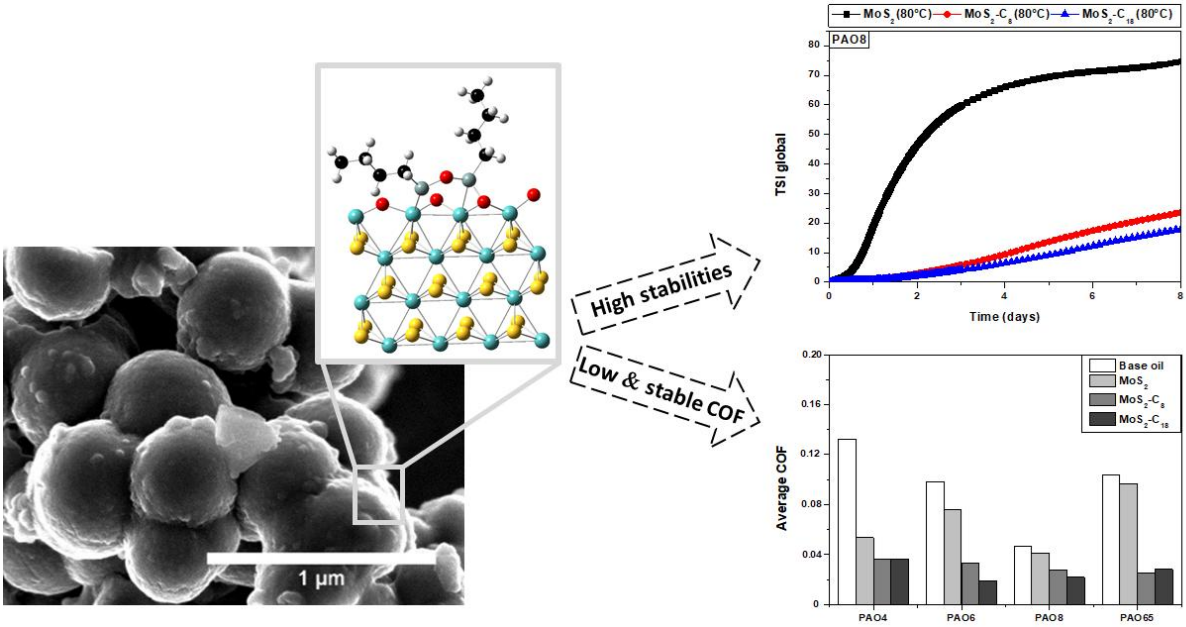

Keywords:

MoS_2 particles, lubricant formulation, alkyltrichlorosilane grafting agents, surface hydrophobization, colloidal stability, friction reduction.

1. Introduction

Wind energy is one of the world's largest and most reliable sources of renewable energy, with an installed capacity of about 600 GW by the end of 2018, and which could exceed 800 GW by 2022, according to GWEC forecast. [1] However, surface and contact damage between moving components, caused by friction and wear phenomena, leads to premature failure of wind turbines components, which increases operating and maintenance costs and reduces therefore its competitiveness. [2.3] For instance, wind turbine gearboxes are designed to

operate for at least 20 years, but most of them can fail after only 5 to 7 years. [4] The cause of these failures is related to severe operating conditions such as high loads and unstable operating conditions, i.e., wind speed, humidity, dust and extreme temperatures. [5] To overcome the rapid deterioration of the surface of moving components, improving lubrication performance and durability is necessary to increase the yield and service time of moving parts of wind turbines, which can improve energy efficiency, reduce maintenance costs and increase reliability. [6,7]

The addition of nanoparticles to the oil significantly improves the tribological properties compared to traditional lubricants. [8] These advanced lubricants could be formulated with transitions metal dichalcogenides, especially MoS_2 and WS_2, considered among the most efficient additives. Their layered structure allows easy sliding while the highly polarized sulfur atoms promote interaction between the particles and the metal surface. [9,10] Such additives improved tribological performances of oils even under severe conditions of high temperature or vacuum. [11,12]

Thus, considerable efforts have been devoted to controlling the morphology and the size of MoS_2 nanoparticles. Various synthesis methods such as hydrothermal, [13] solvothermal, [14] ball milling [15] or CVD [16] can lead to the formation of particles of various morphologies, such as nanosheets, [17] nanospheres, [18] flower-like, [19] nanowires, [20] or nanorods [21]. The tribological behavior of these nano-additives depends on various parameters, such as their shape, size, concentration and crystallinity. Table SI1 presents some examples of average friction coefficient obtained with either coated or bare MoS_2 particles of various morphologies and sizes. For instance, nanometer-size MoS_2 has proven to be more effective in both friction reduction and wear resistance than bulk micrometer-size MoS_2. [22] This could be because the smaller particles are more dispersible and more likely to enter smaller contact angle areas. Furthermore, their high surface area increases their reactivity with rubbed surfaces and facilitates the formation of the tribofilm. Charoo et al [23] have studied the tribological features of 0.5 wt.% and 1 wt.% MoS_2 particles of various sizes (of 35μm, 7μm, 3μm and 90nm) in SAE20W40 lubricant. The study carried out under different loads (of 75N, 100N and 125N) showed that the friction coefficient and the wear volume decrease with the decrease of the particles size. Moreover, poorly crystallized particles were found to further reduce the friction and wear compared to their well-crystallized analogues, probably due to facilitated exfoliation favored by surface defects.[24] Shape is another parameter that might

influence the tribological properties of nano-lubricants, because the contact pressure exerted during loading varies as follows: (i) spherical particles have point contact with the countersurface, (ii) platelets have a plane contact and (iii) sheets have a line contact.[25] Some studies have shown that MoS_2 nanoballs further improve tribological performance in liquid paraffin compared to nano-slices of MoS_2,[26] while others have reported that morphology and size of MoS_2 particles have little or no influence on their tribological performance in poly-α-olefin oil, and that the friction reduction and anti-wear properties of MoS_2 particles are closely related to the contact pressure.[27]

Unfortunately, the use of MoS_2 nanoparticles as lubricant additives is limited by their sedimentation in nonpolar organic media, such as oils. Nanoparticles are characterized by a high and reactive surface area, capable of adsorbing impurities and agglomerating, resulting in an increase in sedimentation rate and hence the loss of their tribological benefits. The aforementioned phenomenon can be avoided by modifying the surface of the nanoparticles. Various dispersants have been proposed to improve the stability of MoS_2 dispersions, but the search for a balance between the amounts of dispersant and additive ensuring the required stability and the high tribological performance remains difficult.

In our previous work [28], the effect of MoS_2 particles morphologies (platelets *vs* spheres) and surface hydrophobization on their colloidal stability was investigated in poly-α-olefins base oils (PAO). We showed that the MoS_2 dispersibility could be increased through alkylsilane grafting on the MoS_2 surface defects (the longer the alkyl chain, the more stable the formulation), and with the increase of the oil kinematic viscosity.

Based on those results, submicrometric hydrophobic spheres of MoS_2 were used as additives in PAO base-oil formulations. Herein, we investigate the tribological properties of the resulting formulations together with the effect of the temperature on the colloidal stability, another important parameter that influences the tribological properties, for temperatures as high as 80°C. Finaly, the nature of the grafting was investigated through combined FT-IR and DFT calculations.

Experimental part

Synthesis of submicron MoS_2 particles

Chemical reagents used in this work were purchased from Sigma Aldrich and were used without further purification.

The synthesis procedure of submicron MoS_2 particles was adapted from a previous study, [29] and was performed in a 35 mL Teflon-lined stainless steel autoclave. Ammonium molybdate (0.0288 g), sulfur powder (0.0091 g), lithium hydroxide (0.205 g), ammonium carbonate (0.0109 g) and hydrazine (0.1 mL) were dissolved in 28 mL of ethylenediamine. The solvothermal treatment was performed at 190°C for 24 h. The autoclave was then cooled down to room temperature and the resultant product was recovered from the solution by centrifugation. The particles were washed several times with acetone and distilled water. Lastly, the black powder obtained was dried under vacuum at 60°C for 3h. The yield was quasi-quantitative.

Surface hydrophobisation of submicron MoS_2 particles

The surface hydrophobization of MoS_2 particles was carried out with two silane derivatives, octadecyltrichlorosilane (ODTS, $C_{18}H_{37}SiCl_3$) and octyltrichlorosilane (OTS, $C_8H_{17}SiCl_3$). 1 wt.% of alkyltrichlorosilane (ODTS or OTS) was added to a dispersion of 0.1 wt.% of MoS_2 particles in poly-α-olefin oil. The mixed solution was ultrasonicated for 15 min (using a 200 W Sonopuls HD 2200 device used at 45% of its nominal power), and then magnetically stirred for 2 h at room temperature.

2.1. Characterisation methods

X-ray diffraction (XRD) was performed using a Bruker D8 ADVANCE ECO diffractometer with Cu/Kα radiation (λ = 0.154 nm) and a scanning rate of 0.04°/s. The morphology of the MoS_2 samples was observed using a Hirox SH-4000M electron microscope equipped with an energy-dispersive X-ray (EDX) spectrometer. XPS analyses were recorded using a KRATOS Axis Ultra X-ray photoelectron spectrometer (Kratos Analytical, Manchester, UK) equipped with a monochromatic Al Kα X-ray source ($h\nu = 1486.6$ eV) operated at 150 W. FTIR analysis was performed on a Jasco 410 spectrometer at a spectral resolution of 4 cm^{-1}.

2.2. DFT calculations

Possible grafting modes of silane derivatives on MoS_2 nanosheets models, [30-32] some of them being oxygenated at their edges, [33,34] have been explored by means of Density Functional Theory (DFT) calculations using the Vienna Ab-initio Simulation Package (VASP).[35] These calculations employed the PAW method,[36,37] and the PBE functional [38] with the D2 correction to account for dispersion forces.[39,40] The plane wave cutoff energy was set to 450 eV and the sampling of the Brillouin-zone was restricted to the Γ-point.

To evaluate our predicted configurations, the vibration frequencies were calculated by numerical differentiation of the force matrix and compared with the FTIR measurements.

2.3. Stability evaluation

PAO base oils were graciously supplied by Chevron Phillips Chemical Company LP (Table SI2). The dynamic viscosity of oils with and without bare and hydrophobized MoS_2 particles was studied with an Anton Paar Physica MCR301 rotational rheometer, equipped with a temperature-measuring device and a coaxial cylinder (CC27). The shear rate was varied from 10 to 1000 s^{-1} and the temperature from 0 to 80°C.

Colloidal stability of suspensions was firstly followed visually; pictures were taken at regular times for all prepared formulations. Furthermore, the effect of temperature on the colloidal stability of prepared formulations was evaluated using a TURBISCAN LAB optical analyser (Formulaction, France), based on a light-scattering detection method. The analysis was carried out on the basis of transmission (T) and backscattering (BS) profiles. Multiple scans were performed at specific times (8 days in total) all along the vertical axis of the tube. Since any destabilisation phenomenon occurring in a suspension has an effect on the intensities of Transmission (T) and/or backscattering (BS) signal over time, the stability evolution as function of time can be followed by so called Turbiscan Stability index (TSI). This parameter simply sums up the evolution of T or BS light at every measured position (h), based on a scan-to-scan difference, over the total sample height (H). It thus reads:

$$\mathrm{TSI} = \frac{\sum_{\mathrm{h}} |\mathrm{scan_i}(h) - \mathrm{scan_{i-1}}(h)|}{H} \qquad (1)$$

The TSI is a single, dimensionless parameter allowing rapid comparison and characterisation of the physical stability of different formulations. The lower the changes of transmission and/or backscattering intensity, the lower the value of TSI and hence the more stable the formulation. For example, destabilisation is visible to the naked eye for TSI values typically higher than 3 (see Figure SI1). Finally, the destabilisation kinetics were obtained by plotting the TSI values as a function of time.

2.4. *Tribological measurements.*

The tribological properties of the prepared lubricants were investigated using a CSM pin-on-disc tribometer. The disc was made of 304L stainless steel, with a diameter of 30 mm and a height of 5 mm. The balls used, 6 mm in diameter, were made of chrome steel type 100C6. The tests were carried out with 1 mL of lubricant at a frequency of 0.1 Hz, with a normal load of 1N and a constant speed of 5 mm/s at 22°C and a humidity of about 34 %.

3. Results and Discussion

3.1. Chemical and morphological characterisation of MoS_2 particles

The size and morphology of MoS_2 thus synthesised were determined by SEM (Figure 1 a, b). The particles have a spherical shape with a diameter of about 300 to 500 nm. Moreover, some smaller particles can be distinguished on SEM images. They may be due to the rapid nucleation process and incomplete growth in favour of larger and more stable particles. [29, 41]

X-ray diffraction patterns of synthesised MoS_2 (Figure 1c) show broad peaks, characteristic of poorly crystallised molybdenum disulphide, compared to hexagonal 2H-MoS_2 (JPCD 37-1492). The diffraction peak at about 15° is attributed to the (002) plane of hexagonal MoS_2, indicating the stacking of MoS_2 layers. The diffraction peaks observed at 37.3°, 48° and 58.3° can be attributed to (103), (105) and (110) planes, respectively. Furthermore, the less intense peak observed at about 9.1° indicates an expansion of the interlayer distance of MoS_2, from 0.61 nm to 0.96 nm. This could be due to the intercalation of atoms or ions such as oxygen or ammonium [42,43] originating from the precursors. Interlayer expansion is expected to weaken van der Waals forces between adjacent layers of MoS_2, facilitating their exfoliation, [44,45] and thus contributing to the improvement of their tribological performances.

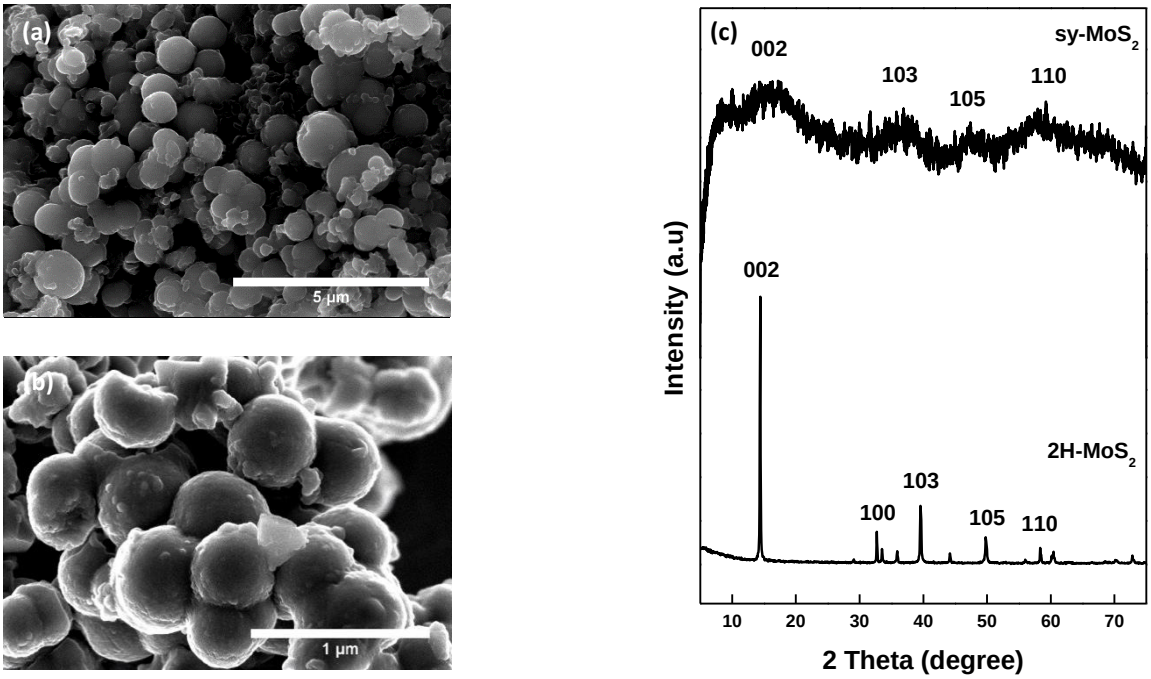

Figure 1. (a,b) SEM images of MoS_2 particles synthesised here, and (c) XRD patterns of synthesised MoS_2 and 2H-MoS_2 given for comparison.

XPS analysis was performed to investigate the chemical composition and the valence states of the MoS_2 particles. The survey data (Fig. 2 a) indicate the presence of Si, S, Mo, C and O at the surface of the sample (MoS_2-C18). The Mo 3d spectrum (Fig. 2 b) displays four peaks with two strong ones at 231.7 and 228.8 eV that can be associated with Mo $3d_{3/2}$ and Mo $3d_{5/2}$ doublets of Mo^{4+}. [46] The peak at 225.7 eV is assigned to S 2s. The peak at 234.7 eV can be attributed to Mo $3d_{5/2}$ of Mo^{6+}. Both valence states, Mo^{6+} and Mo^{4+}, are expected in MoS_2 particles which exhibit six-fold coordinated Mo-atoms at the M-edge and at the S-edge the fourfold coordinated Mo-atoms. [30,33] An additional peak at about 168 eV in the S 2p spectrum (Fig. 2b), suggests the existence of SO_4^{2-} [47], also observed by FTIR at about 1040 cm^{-1} (Fig. 3a). The S 2p spectrum shows two other peaks observed at 162.8 and 161.3 eV corresponding to S $2p_{1/2}$ and S $2p_{3/2}$ of S^{2-}, respectively [48] which are in good agreement with the values reported for MoS_2 particles. [49,50] The Si 2p spectrum exhibits two peaks at 101.7eV and 102.2eV that could be assigned to Si-C and Si-O, respectively, and indicating thus the grafting of alkyl-silane on the surface of MoS_2 particles.

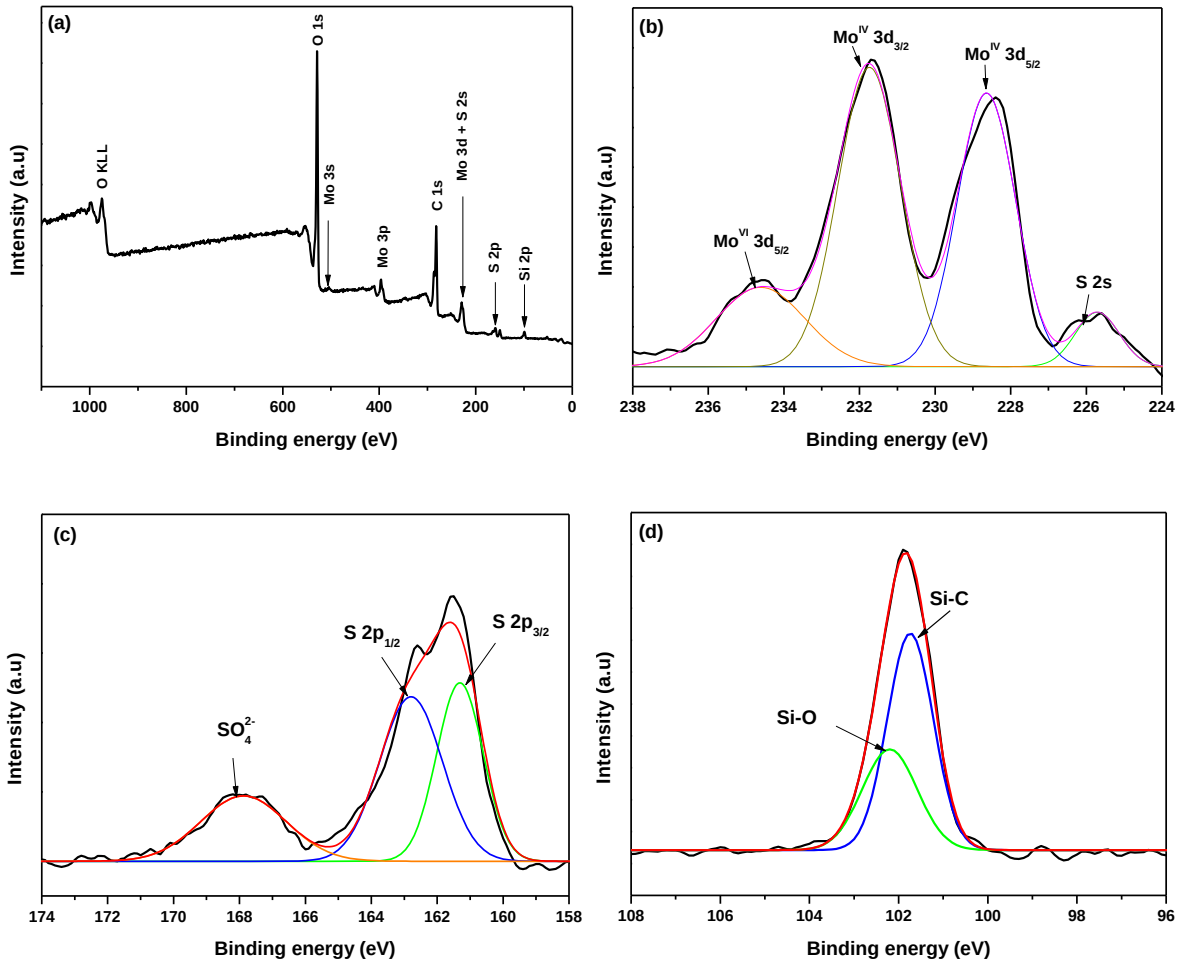

Figure 2. XPS spectra of MoS_2–C18: (a) Survey date, (b) Mo 3d, (c) S 2p and (d) Si 2p.

Further insights on the chemical structure of the materials were gather from FTIR measurements and DFT calculations. The formation of Mo-S bonds was confirmed by the presence of characteristic elongation frequencies, computed in the range of 410-430 cm^{-1} and experimentally observed at 420 cm^{-1}. As all computed DFT frequencies for the bare MoS_2 models appear under 500 cm^{-1}, the vibrations detected above this limit correspond to other chemical bonds. For instance, the band at 1432 cm^{-1} can be ascribed to the ammonium ions from the reagents and responsible of the expansion of the interlayer distance of MoS_2, while the peak at about 3224 cm^{-1} could come from the water adsorbed on the surface of the particles. IR spectrum of bare MoS_2 particles (Fig. 3a) also shows one band at around 490 cm^{-1} that can be assigned to Mo-O bonds, in agreement with the computed characteristic frequencies found at 465, 477, 548, 573 and 607 cm^{-1}. This suggests that a partial sulphur-oxygen exchange reaction might take place at the edges of MoS_2, probably due to the presence of water. [33,34] More importantly, compared to bare MoS_2, three main additional bands appear on both experimental and theoretical spectra of silane-grafted particles (MoS_2-C_8 and MoS_2-C_{18}), at about 3000 cm^{-1} for C-H deformation, 1400 cm^{-1} for Si-C and 1100 cm^{-1} for Si-O, respectively. The assignment of these bands is also in agreement with the calculated ones, confirming thus, that the alkylsilane moieties are covalently bound to MoS_2 through Mo-O-Si(-Alk) linkages. Moreover, the elongations frequencies of Mo-O bonds interacting with silane groups were computed at higher values compared to the one non interacting with silane groups, in the 573-648 cm^{-1} region. They appear on the experimental spectra at around 615 cm^{-1}, as it can be seen on Figure 3a. Overall, among the different configurations tested by DFT, that presented in Figure 3b provides the best agreement between experimental and calculated frequencies. We limit ourselves to the C4 groups instead of C8 or C18 because the corresponding C-H frequencies are rather the same for both species, and the vibrations of the Si-C bond are not affected by the Cn groups located at 2 or 3 Å away.

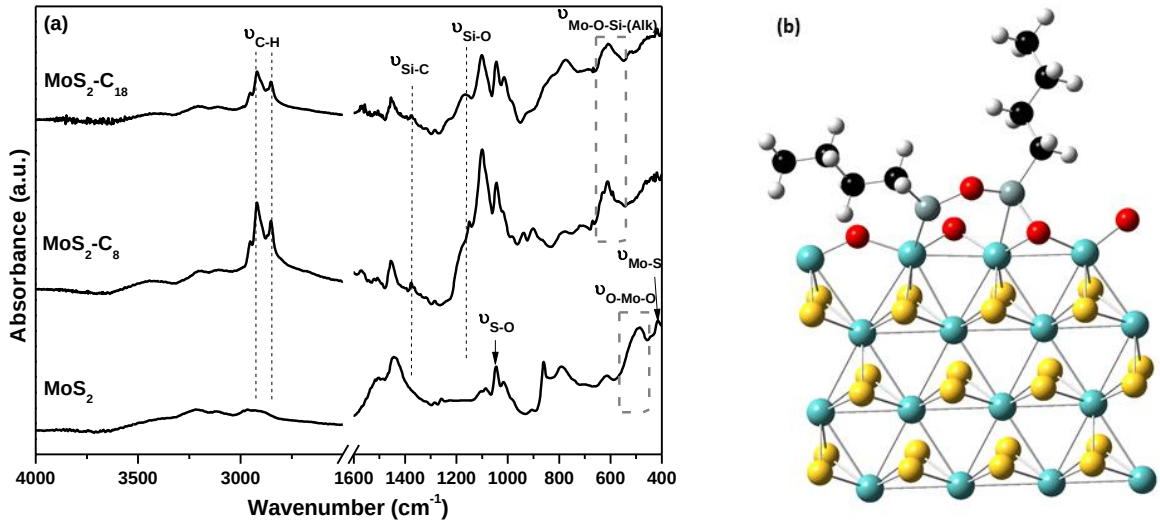

Figure 3. (a) FTIR spectra of bare and hydrophobised synthesised MoS_2 particles and (b) Scheme of silane-grafted MoS_2, oxygenated at the edge through C-Si and Si-O bonds, based on the comparison between experimental and DFT frequencies. Colour code: S in yellow, Mo in blue, O in red, Si in grey, C in black, H in white.

3.2. Colloidal stability of bare and functionalized MoS2 particles in poly-α-olefin oils

All formulations were obtained by dispersing 0.1 wt.% of MoS_2 particles (bare or functionalized with 1 wt.% of alkylsilane) in poly-α-olefins. Three oils of relatively low dynamic viscosities were selected, PAO4, PAO6 and PAO8 (32, 60 and 90 mPa·s at 25°C, respectively), as well as a highly viscous oil, PAO65 (1650 mPa·s at 25°C). All oils are oligomers of 1-decene ($C_{10}H_{20}$) and vary in their polymerization degree. PAO4 is a tetramer, PAO6 is a hexamer and PAO8 is an octamer, while PAO65 is a polymer (of unknown molecular formula).

First, the dynamic viscosity of the oils, with or without MoS_2-based additives, was determined as a function of temperature, up to 80°C (Figure 4). For example, the values of the dynamic viscosity (with or without particles) ranged from 7 mPa·s for PAO4 at 80°C to 1630 mPa·s for PAO65 at 25°C. A selection of values is presented in Table SI2. Whatever the oil, there is a decrease in the dynamic viscosity with the increase in temperature, which is a typical behavior of Newtonian liquids. Indeed, even if the transfer of molecular momentum between the molecules increases with their kinetic energy, the cohesion force decreases with the increase of the temperature as the molecules move away. The graphs show that, regardless of oil or temperature, the MoS2-based additives do not alter the Newtonian behavior of the

pristine PAO oils, nor their dynamic viscosity. This finding is readily explained by the very low concentration at which the MoS2 particles have been added, 0.1 wt.%.

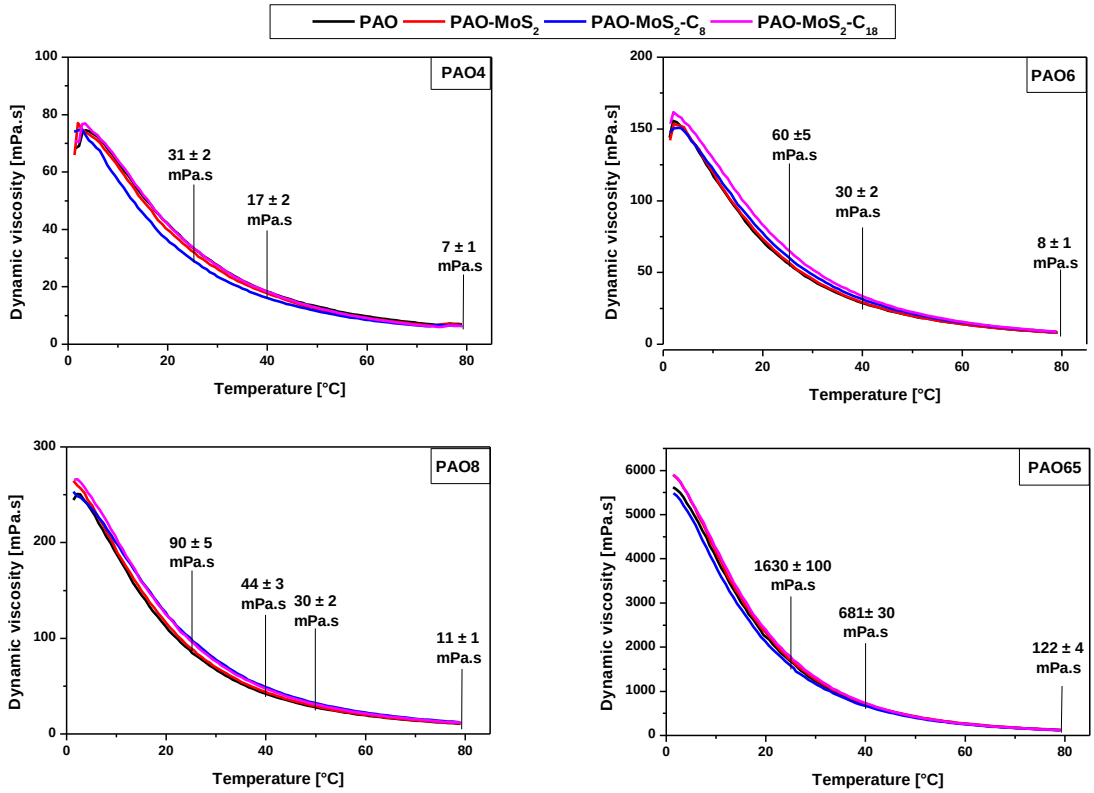

Figure 4: Evolution of the dynamic viscosity of PAO lubricants, without or with MoS_2-based additives, as a function of temperature, in the range from 0 to 80°C.

On the contrary, the stability of the dispersions was significantly influenced by the addition of particles, as shown by Turbiscan measurements. From the variation rate of transmitted and backscattered intensities with respect to the initial point (see a selected example in Fig. SI2), the Turbiscan Stability Index (TSI) can be determined. A high stability index is obtained when the variations between the transmission and/or the backscattering intensity are high and, therefore, the higher is the TSI, the lower is the stability of the dispersions. According to the manufacturer of the Turbiscan device, the TSI scale is such that values of 0 to 0.5, 0.5 to 1, 1 to 3, 3 to 10 and higher than 10 correspond to extremely stable, stable, moderately stable, poorly stable and unstable formulations, respectively (Figure SI1).

The evolution of the TSI as a function of the natures of oils and additives at 25°C is given in Fig.5, while those at 40 and 80°C are given in Fig. SI 3-4. All formulations contained the same amount of additive, 0.1 wt.%. In general, the colloidal stability increased with the

viscosity of the oils and with the chain length of the grafted alkylsilane, the most stable suspensions being obtained with the particles coated with ODTS. For example, after 4 days of rest at 25°C, the TSI of formulations containing pristine particles decreased as the viscosity increased from 55 for PAO4 to 12 for PAO6, to 2.5 for PAO8 and to 0.6 for the most viscous one, PAO65. By increasing the temperature, the viscosity of the oils decreased and, therefore, the stability of the formulations decreased. For instance, the TSI values for bare MoS_2/PAO8-base oils increased after 4 days from 2.5 at 25°C to 65 at 80°C.

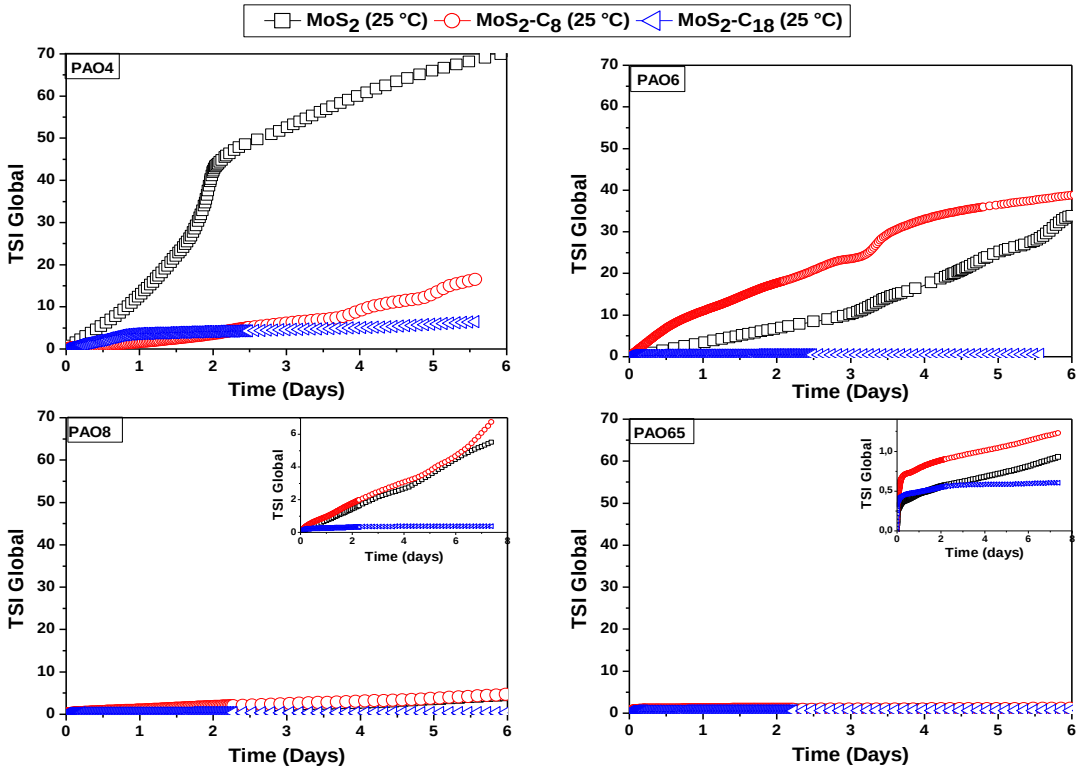

Figure 5. Evolution of Turbiscan Stability Index (TSI) of the suspensions at 25°C. The insets are zooms on the first part of the curves, justified by the low values of TSI.

The TSI results at higher temperatures generally indicate that the stability decreases as the temperature increases from 25°C to 80°C. This is due to increased thermal motions, thereby increasing the rate of molecular collision rate, decreasing the viscosity, and thus increasing the rate of sedimentation and the clarification of the suspension with time. Concerning the thermal stability of the formulations prepared with hydrophobized MoS_2, the TSI data reveal that the most stable suspensions along the time are obtained with the particles coated with ODTS, since the TSI values are smaller than 1 up to 40°C with all kind of lubricant, except for PAO4 at 25°C (see blue curves on Fig. SI 3-4). At 80°C, the loss of stability of the MoS_2-

C18 modified particles seems to be counterbalanced only in PAO65 oil that presents the highest dynamic viscosity value (around 121 mPa·s).

Figure 4 has shown that the dynamic viscosity values of the suspensions based on PAO4 at 25°C are almost equivalent to those of the suspensions based on PAO6 at 40°C (around 30 mPa·s) and to those of PAO8 near 50°C. The values are of about 30 mPa·s. Comparing the TSI values obtained for PAO4 at 25°C with those of PAO6 at 40°C and with the interpolated value of PAO8 at 50°C, one can estimate the evolution of the Turbiscan stability index as a function of the used dispersants, at a constant viscosity of 30 mPa·s (Figure 6). Thus, it appears that the stability of the formulations containing bare particles significantly increases with the increase of the polymerization degree of the oil, from PAO4 to PAO6 and to PAO8. The same trend, but with less pronounced variation is observed for C8 (OTS)-coated particles, while stability remains constant for the formulations based on C18 (ODTS)-coated particles. This could be due to the molecular environment of MoS_2 particles. The higher the hydrophobicity of the particles, the higher the compatibility with the oil and, consequently, the higher is the stability of the formulation, regardless of the viscosity of the oil.

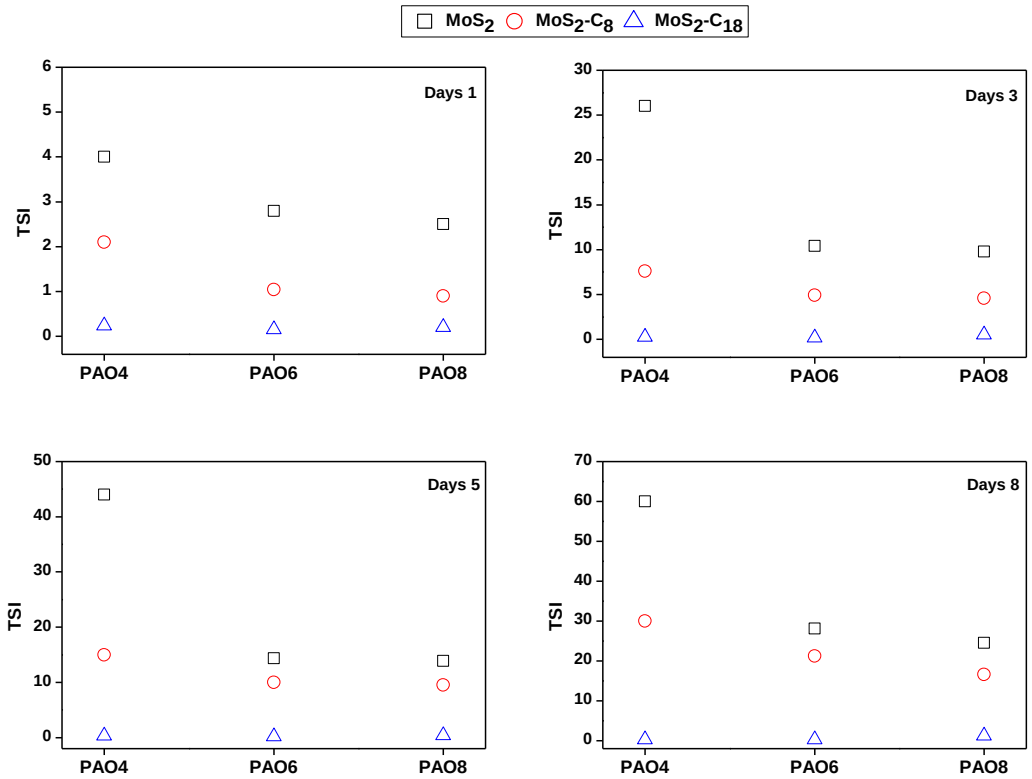

Figure 6. Stability evolution of suspensions based on PAO4, PAO6 and PAO8 at constant viscosity, of 30 mPa·s.

3.3. Tribological properties of bare and functionalized MoS2 particles dispersed in PAO base oils.

The first tribological tests were performed on bare MoS_2 particles to determine the minimum concentration required to ensure maximum reduction of the friction coefficient. To do this, the study was carried out on the least viscous oil (PAO4, dynamic viscosity of about 33 mPa·s at 25 °C) and which presents more disturbances according to the stability tests. The concentration of particles was varied from 0, 0.1, 0.5 to 1wt%. Figure 7 shows the evolution of the friction coefficient for PAO4 as a function of the concentration of MoS_2 particles.

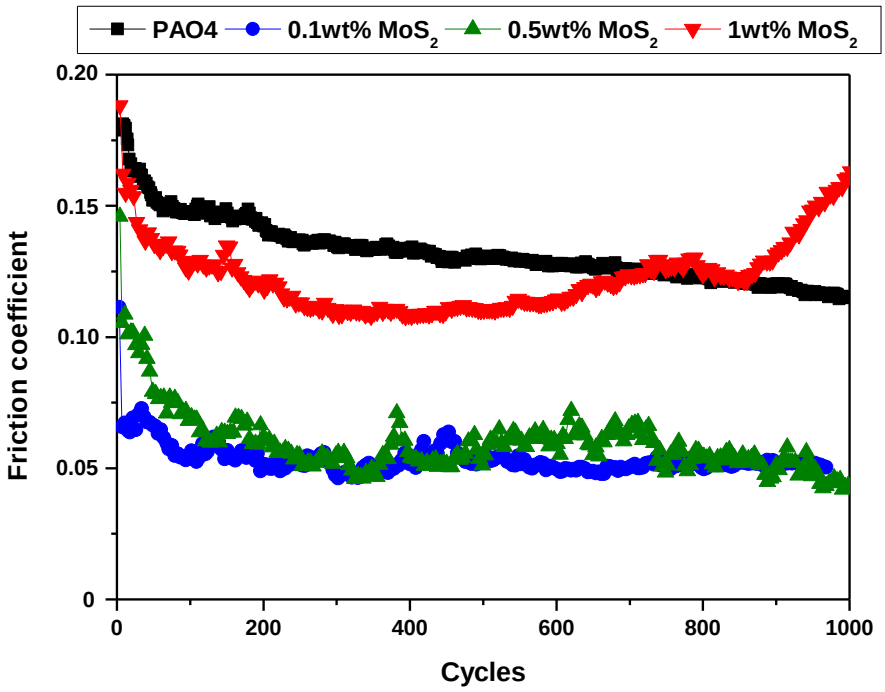

Figure 7. Friction coefficient as a function of the concentration of MoS_2 particles.

Under these operating conditions, the reference test for pure PAO4 oil produces a friction coefficient of 0.18 at the beginning of the test, which decreases to 0.15 over the first 200 cycles. Then, it tends to stabilize between 0.14 and 0.11. The addition of 0.1 and 0.5 wt.% MoS_2 results in a significant reduction in the coefficient of friction compared to the pristine oil, reaching values as low as 0.05. On the contrary, the addition of 1 wt.% of MoS_2 particles resulted in a slight decrease in the friction coefficient during the first 800 cycles, and then a continuous increase until the values of pure base oil were exceeded (0.18). This behavior can be justified by the aggregation and sedimentation phenomena of the MoS_2 particles, which prevent their penetration into the contact area and therefore limit their presence between the moving surfaces.

In conclusion, under our experimental conditions, the optimum concentration of MoS_2 additives leading to better friction-reducing properties is 0.1 wt%. By increasing the concentration of MoS_2 particles, the coefficient of friction increased, which clearly indicates that an excess of particles promotes their agglomeration and causes their sedimentation, which limits the number of particles present between the surfaces in contact and consequently prevents the formation of the tribofilm in the contact area, ultimately leading to the loss of their lubricating efficiency.

Once the concentration was set, we studied the influence of the oil viscosity and of the chain length of the dispersant on the friction coefficient. The results are presented in Figure 8.

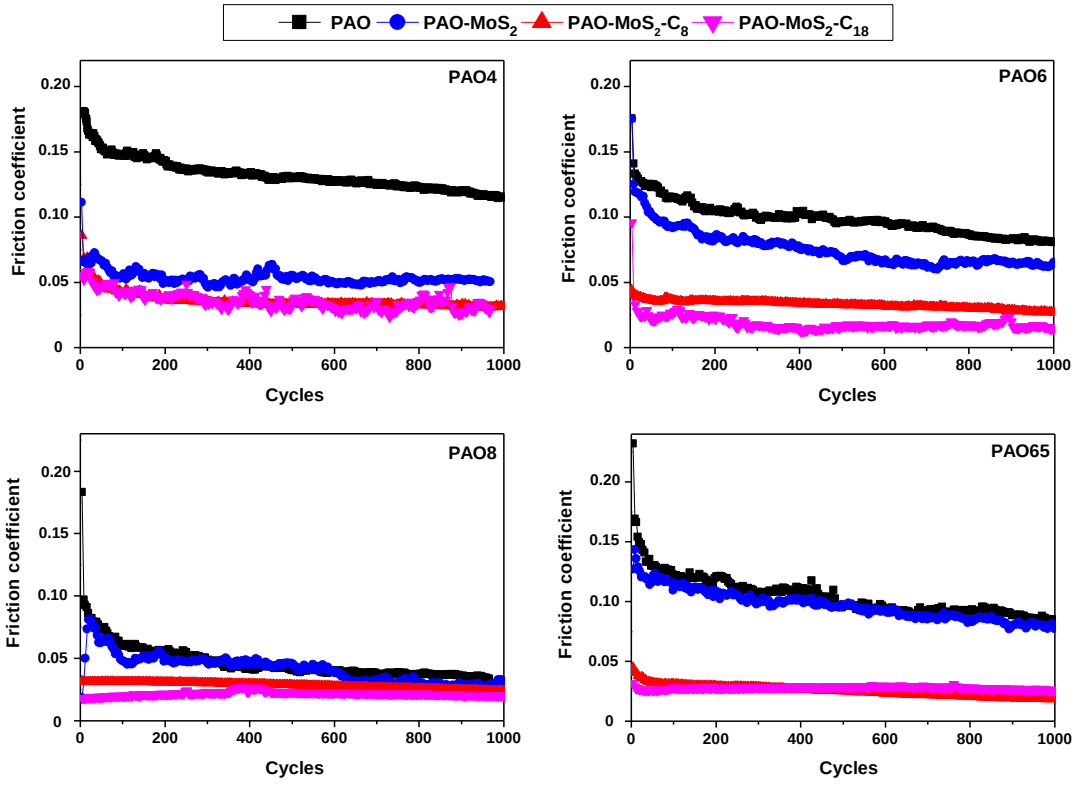

Figure 8. Friction coefficient of bare and functionalised MoS_2 particles at 0.1 wt.% in PAO base oils.

The average coefficients of friction obtained for each oil are illustrated in Figure 9. Compared to the pure PAO oils, the addition of 0.1 wt.% of MoS_2 particles allowed a significant reduction in the friction coefficient for the four types of PAO oils. Nevertheless, the friction reduction capabilities of MoS_2 decreased with increasing viscosity of PAO oils, especially in PAO8 and PAO65 where the addition of bare MoS_2 only produced a slight improvement in friction coefficients compared to pure base oil.

On the other hand, the lubricants containing MoS_2 submicroparticles modified with alkylsilane dispersants produced the lowest friction coefficients in the four PAO base oils. This observation can be justified by their high stability and dispersibility, provided by the hydrocarbon chains of the dispersant which reduce their agglomeration and sedimentation rates. As a result, their displacement to the contact area is facilitated, where they react with the metal surfaces and form a protective lubricant film layer based on MoS_2 particles. This might consequently prevent direct contact between the metal surfaces of the ball and the disc.

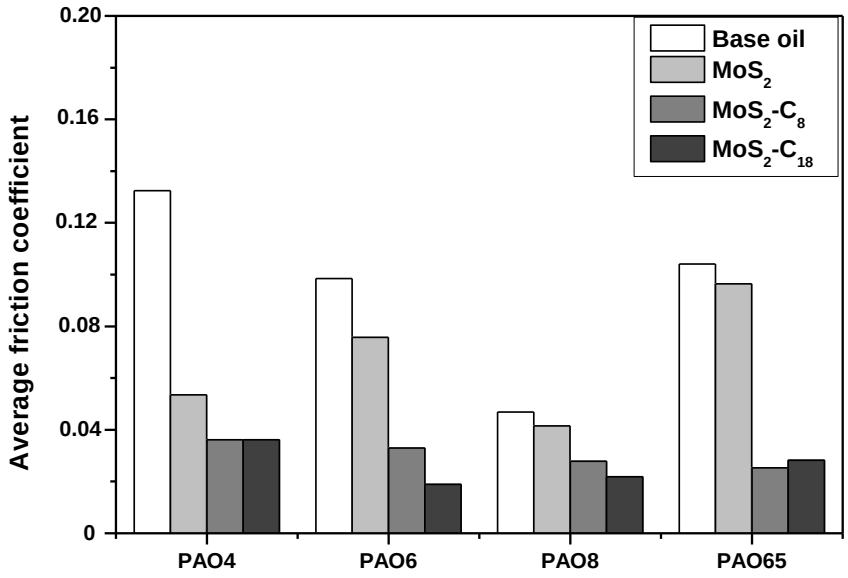

Figure 9. Average friction coefficient in PAO base oils containing 0.1 wt% of MoS_2 particles.

The average coefficients of friction calculated for each formulation show the high lubricating power of the MoS_2 submicroparticles relative to the base oil alone, and especially after the hydrophobization of their surfaces by alkyltrichlorosilanes. The use of MoS_2 particles as additives resulted in a reduction in friction of about 60%, 23%, 12% and 7% compared to pristine PAO4, PAO6, PAO8 and PAO65, respectively. The surface modification of these particles with alkyl-silane groups allowed a further reduction of up to 70% for PAO65 over the genuine oil. The lowest friction coefficients, between 0.02 and 0.03, were obtained with C18- grafting.

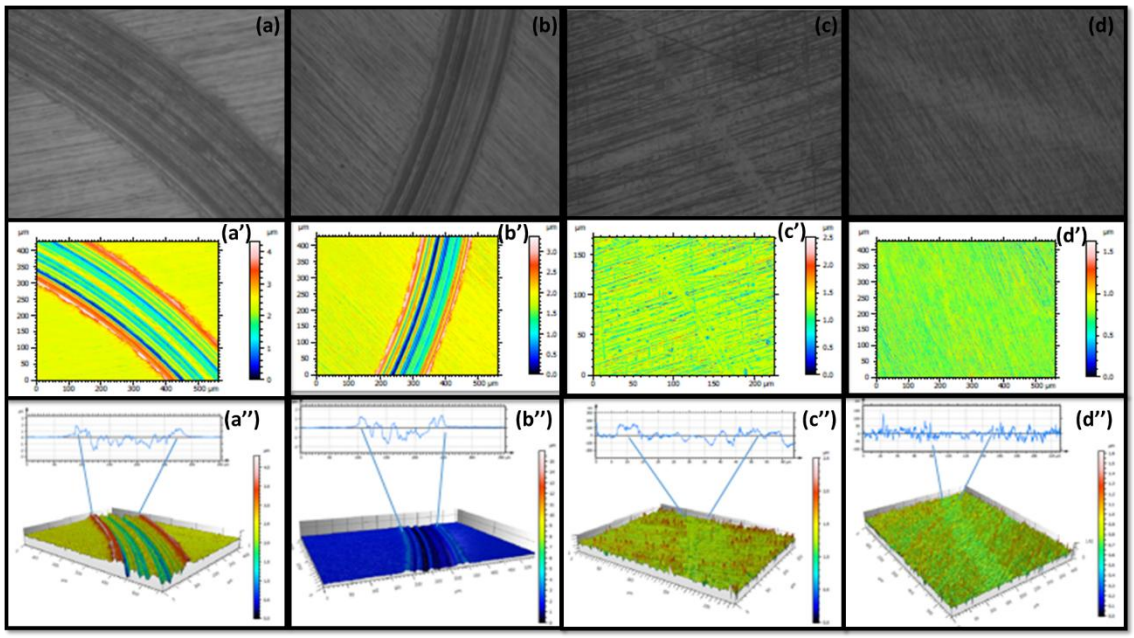

Figure 10. Optical micrographs, pseudo-color view, 3D view and profile curve of wear scar: (a, a', a'') PAO4, (b, b', b'') PAO4/MoS_2, (c, c', c'') PAO4/MoS_2-C8, (d, d', d'') PAO4/MoS_2-C18.

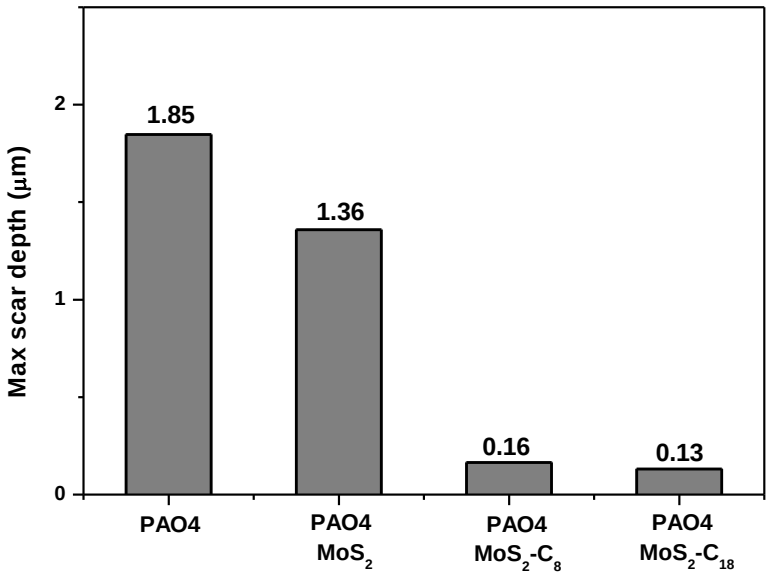

Figure 11. Maximum scar depth obtained with different formulations in PAO4.

The evaluation of the wear scar obtained for the different formulations in PAO4 after the friction tests is given in Figures 10 and 11. The images indicate that the addition of the bare MoS_2 particles present a slight reduction in the wear track compared to that obtained with the

PAO4 without MoS_2. More important, the wear traces were considerably reduced with the formulations containing hydrophobised MoS_2 particles. The addition of 0.1wt% of grafted particles to the PAO4 have shown the best anti-wear performance and led to surfaces with almost no signs of wear as shown in Fig.10. The maximum wear depth (Fig. 11) obtained for the lubricant based on MoS_2-C8 is 0.165 μm, compared to around 1.35 μm in the case of bare MoS_2 formulations and 1.85 μm obtained for free PAO4. This represents a decrease of more than 91% instead of 26% obtained with bare MoS_2. This value decreased further to reach more than 92.5% (0.13 μm), while using a formulation containing 0.1wt% MoS_2-C18 additives.

The friction mechanisms of these submicron MoS_2 particles could be explained by several factors. It has already been shown that, for spherical and IF-MoS_2 particles, the ultra-low friction coefficient is related to their mechanisms of rolling, deformation and easy exfoliation,[52,53] favored by their lamellar and poorly crystallized structure.[54] It is described that the formation of tribofilm for IF-MoS_2 requires three steps: i- the passage of particles within the contact area, ii- the exfoliation of the IF-MoS_2 nanoparticles under the pressure and the shear applied by the rubbing surfaces, creating free MoS_2 layers in the contact area, and iii- tribochemical reaction between the MoS_2 layer and the steel surfaces, thus creating a protective film all over the contact area. [55] The chemical characterization of the tribofilm formed in the contact area of steel surface indicates the presence of Mo-O, S-O and Fe-O bonds, in addition to characteristics MoS2 bonds, suggesting that the attachment of MoS_2 particles to the surface of steel can be achieved by the (tribo) chemical reaction between exfoliated MoS_2 layers and iron oxide coming from the steel surface.[56,57] This proves that a partial oxidation of the surface could be beneficial because it could facilitate the adhesion of particles to the surface of the steel.

In the case of modified MoS_2 particles, the ultra-low friction coefficient is attributed to their high dispersion and the absence of agglomerates, which facilitate their introduction and their passage in the contact area. The small particles can then stack and fill the micro-pits and the damaged parts produced by the wear of the contact surface, and thus allow the formation of a protective film. This makes the surface relatively flat and significantly improves the tribological properties of the PAO base oil.

Conclusion

The studied MoS_2 particles were obtained following a solvothermal method yielding to individualized spheres of about 400 nm with a poorly crystallized structure. The compatibility between the hydrophilic surface of MoS_2 and hydrophobic PAO oils was enhanced by coating the surface of the submicroparticles with alkylsilanes presenting two chain lengths; octyl and octadecyl. FTIR measurements combined with DFT calculations suggested sulfur-oxygen exchange on the MoS_2 edge surfaces during the synthesis and covalent grafting of alkylsilanes through Mo-O-Si(-Alk) bonds. Furthermore, it was found that the grafting chain can increase significantly the colloidal stability and the longer was the chain length, the more stable were the formulations. Extremely stable formulations (TSI < 0.5) were obtained with octadecyl grafting in all oils. On the other hand, it is known for liquids that the viscosity and the stability of the formulations decreased upon heating. Nevertheless, the formulation in highly viscous PAO65, interestingly, remained very stable even at 80°C (TSI < 1), and was also influenced by the type of the used oil. For example, for a given hydrophobic agent and oil viscosity (i.e., of about 30 mPa·s corresponding to PAO4 at 25°C, PAO6 at 40°C and PAO8 at 50°C), the stability increased with the polymerization degree of the oil and thus with the its hydrophobicity.

Regarding the tribological behavior, the involved film seems to be influenced not only by the oil viscosity but also the hydrophobization of MoS_2 additives. Again, octadecyl grafting was found to be the most efficient with respect to friction coefficient reduction to 0.02. This is apparently attributed to their highly dispersive effect allowing reduction of both the size and agglomeration rate of particles in the PAO base oil, which help their penetration within the contact area.

As compared with the commonly commercial dispersants/surfactant used in formulated industrial oils, such as PIBS, which is found to negatively affect, under certain conditions, the tribological performance of the additives used.[54,58] Herein, the studied dispersants based on alkyl-silane groups proved their efficiency with respect to colloidal stability and triblogical performance, which may paves the way for application in industrial oils as dispersant, suitable for operating under severe climate conditions. As further perspectives, the effect of superhydrophobicity of antifrictional properties should be considered.

Acknowledgements

The authors thank the institute IRESEN/ Morocco (Project Innowind13 Nanolubricant) for its financial support and for the scholarship awarded to MZS. AP thanks Dr. E.-E. Bendeif (CRM2, University of Lorraine) for performing X-ray measurements and A. Renard and Dr. M. Mallet (LCPME, University of Lorraine) for performing XPS measurements. AP also thanks P.L. Marande for engineering steel disks for friction measurements. P. Gadonneix (IJL, University of Lorraine) is thanked for performing Turbiscan measurements.

References

[1] Global Wind Energy Council, Global wind report annual market update (2017).

[2] R. Errichello, S. Sheng, J. Keller, A. Greco, Wind Turbine Tribology Seminar - A Recap, United States (2012), doi:10.2172/1036041.

[3] K. Sayfidinov, S.D. Cezan, B. Baytekin, H.T. Baytekin, Minimizing friction, wear, and energy losses by eliminating contact charging, Sci. Adv. 4 (11) (2018) eaau3808, doi:10.1126/sciadv.aau3808.

[4] J.V. Rensselar, Extending wind turbine gearbox life with lubricants, Tribol. Lubr. Technol. 69 (5) (2013) 40-48.

[5] C. Nutakor, D. Talbot, A. Kahraman, An experimental characterization of the friction coefficient of a wind turbine gearbox lubricant, Wind. Energy 22 (4) (2019) 509-522, doi:10.1002/we.2303.

[6] T. Haque, S. Korres, J. T. Carey, P.W. Jacobs, J. Loos, J. Franke, Lubricant effects on white etching cracking failures in thrust bearing rig tests, Tribol. T. 61 (6) (2018) 979-990, doi: 10.1080/10402004.2018.1453571.

[7] D. Coronado, J. Wenske, Monitoring the oil of wind-turbine gearboxes: Main degradation indicators and detection methods, Machines 6 (2) (2018) 25, doi:10.3390/machines6020025.

[8] E. Omrani, P. Menezes, P. Rohatgi, Effect of micro- and nano-sized carbonous solid lubricants as oil additives in nanofluid on tribological properties, Lubricants 7 (3) (2019) 25, doi:10.3390/lubricants7030025.

[9] Z. Chen, Y. Liu, S. Gunsel, J. Luo, Mechanism of antiwear property under high pressure of synthetic oil-soluble ultrathin MoS_2 sheets as lubricant additives, Langmuir 34 (4) (2018) 1635-1644, doi:10.1021/acs.langmuir.7b03851.

[10] X. Wu, K. Gong, G. Zhao, W. Lou, X. Wang, W. Liu, Surface modification of MoS_2 nanosheets as effective lubricant additives for reducing friction and wear in poly-α-olefin, Ind. Eng. Chem. Res. 57 (23) (2018) 8105-8114, doi:10.1021/acs.iecr.8b00454.

[11] T. Gradt, T. Schneider, Tribological Performance of MoS_2 Coatings in Various Environments, Lubricants 4 (3) (2016) 32, doi:10.3390/lubricants4030032.

[12] K. Gong, X. Wu, G. Zhao, X. Wang, Nanosized MoS_2 deposited on graphene as lubricant additive in polyalkylene glycol for steel/steel contact at elevated temperature, Tribol. Int. 110 (2017) 1-7, doi:10.1016/j.triboint.2017.01.024 .

[13] L. Luo, M. Shi, S. Zhao, W. Tan, X. Lin, H. Wang, F. Jiang, Hydrothermal synthesis of MoS_2 with controllable morphologies and its adsorption properties for bisphenol A, J. Saudi Chem. Soc. 23 (6) (2019) 762-773, doi:10.1016/j.jscs.2019.01.005.

[14] M. Yi, C. Zhang, The synthesis of two-dimensional MoS_2 nanosheets with enhanced tribological properties as oil additives, RSC Adv. 8 (17) (2018) 9564-9573, doi:10.1039/c7ra12897e.

[15] H. Wu, X. Li, X. He, J. Lu, L. Wang, B. Zhou, G. Dong, An investigation on the lubrication mechanism of MoS_2 nanoparticles in unidirectional and reciprocating sliding point contact: The flow pattern effect around contact area, Tribol. Int. 122 (2018) 38-45, doi:10.1016/j.triboint.2018.02.013.

[16] C. Yang, B. Wang, Y. Xie, Y. Zheng, C. Jin, Synthesis of MoS_2 nanoribbons derived from their flake counterparts on graphene substrate by chemical vapor deposition, Nanotechnology 30 (2019), doi:10.1088/1361-6528/ab0a1d.

[17] P. Wu, W. Li, T. Ge, Y. Feng, Z. Liu, Z. Cheng, Preparation and tribological properties of chemically decorated MoS_2 nanosheets with oleic diethanolamide, Lubr. Sci. 31 (1-2) (2018) 41-50, doi:10.1002/ls.1444.

[18] Z. Zhang, P. Wang, F. Wang, Y. Li, W. Lu, X. Jiang, Controlling dispersion and morphology of MoS_2 nanospheres by hydrothermal method using SiO2 as template, Chinese J. Chem. Eng. 26 (5) (2018) 1229-1234, doi:10.1016/j.cjche.2017.12.016.

[19] A. Wang, K. Hu, Y. Liu, R. Li, C. Ye, Z. Yi, K. Yan, Flower-like MoS_2 with stepped edge structure efficient for electrocatalysis of hydrogen and oxygen evolution, Int. J. Hydrogen Energ. 44 (13) (2019) 6573-6581, doi:10.1016/j.ijhydene.2019.01.200.

[20] Y. Jia, Y. Ma, Y. Lin, J. Tang, W. Shi, Facile synthesis of branched MoS_2 nanowires, Chem. Phys. 513 (2018) 209-212, doi:10.1016/j.chemphys.2018.08.019.

[21] C. Wang, H. Wang, Z. Lin, W. Li, B. Lin, W. Qiu, Y.Quan, Z. liu, S. Chen, In-situ synthesis of edge-enriched MoS_2 hierarchical nanorods with 1T/2H hybrid phases for highly efficient electrocatalytic hydrogen evolution, Cryst. Eng. Comm. 21 (12) (2018) 1984-1991, doi:10.1039/c9ce00159j.

[22] K.H. Hu, X.G. Hu, Y.F. Xu, F. Huang, J.S. Liu, The effect of morphology on the tribological properties of MoS_2 in liquid paraffin, Tribol. Lett. 40 (1) (2010) 155-165, doi: 10.1007/s11249-010-9651-z.

[23] M.S. Charooa, M.F. Wanib, M. Haniefc, M.A. Ratherd, Tribological properties of MoS_2 particles as lubricant additive on EN31 alloy steel and AISI 52100 steel ball, Mater. Today. Proc. 4 (9) (2017) 9967-9971, doi:10.1016/j.matpr.2017.06.303.

[24] W. Dai, B. Kheireddin, H. Gao, H. Liang, Roles of nanoparticles in oil lubrication, Tribol. Int. 102 (2016) 88-98, doi:10.1016/j.triboint.2016.05.020.

[25] M. Akbulut, Nanoparticle-based lubrication systems, J. Powder Metall. Min. 1 (1) (2012), doi:10.4172/2168-9806.1000e101.

[26] K.H. Hu, X.G. Hu, Y.F. Xu, F. Huang, J.S. Liu, The effect of morphology on the tribological properties of MoS_2 in liquid paraffin, Tribol. Lett. 40 (1) (2010) 155-165, doi:10.1007/s11249-010-9651-z.

[27] D. Maharaj, B. Bhushan, Nanomechanical behavior of MoS_2 and WS_2 multi-walled nanotubes and carbon nanohorns, Sci. Rep. 5 (1) (2015), doi:10.1038/srep08539.

[28] M.Z. Saidi, H. Akram, O. Achak, C. El Moujahid, A. El Mouakibi, N. Canilho, C. Delgado- Sánchez, A. Celzard, V. Fierro, A. Pasc, T. Chafik, Effect of morphology and hydrophobization of MoS_2 microparticles on the stability of poly-α-olefins lubricants, Colloid. Surface A 572 (2019) 174-181, doi:10.1016/j.colsurfa.2019.04.003.

[29] H. Akram, C. Mateos-Pedrero, E. Gallegos-Suárez, N. Allali, T. Chafik, I. Rodriguez-Ramos, A.G. Ruiz, Low solvothermal synthesis and characterization of hollow nanospheres molybdenum sulfide, J. Nanosci. Nanotechnol. 12 (8) (2012) 6679-6685, doi:10.1166/jnn.2012.4561.

[30] J.-F. Paul, S. Cristol, E. Payen, Computational studies of (mixed) sulfide hydrotreating catalysts, Catal. Today 1 (15) (2008) 139-148, doi:10.1016/j.cattod.2007.07.020.

[31] M. Badawi, J.-F. Paul, S. Cristol, E. Payen, Guaiacol derivatives and inhibiting species adsorption over MoS_2 and CoMoS catalysts under HDO conditions: A DFT study, Catal. Commun. 12 (10) (2011) 901-905, doi:10.1016/j.catcom.2011.02.010.

[32] M. Badawi, J.-F. Paul, E. Payen, Y. Romero, F. Richard, S. Brunet, A. Popov, E. Kondratieva, J.-P. Gilson, L. Mariey, A. Travert, F. Maugé, Hydrodeoxygenation of phenolic compounds by sulfide (Co)Mo/Al_2O_3 catalysts, a combined experimental and theoretical study, Oil Gas Sci. Technol. – Revue d'IFP Energies Nouvelles, 68 (5) (2013) 829-840, doi:10.2516/ogst/2012041.

[33] M. Badawi, J.-F. Paul, S. Cristol, E. Payen, Y. Romero, F. Richard, S. Brunet, D. Lambert, X. Portier, A. Popov, E. Kondratieva, J.M. Goupil, J. El Fallah, J.P. Gilson, L. Mariey, A. Travert, F. Maugé, Effect of water on the stability of Mo and CoMo hydrodeoxygenation catalysts: A combined experimental and DFT study, J. Catal. 282 (1) (2011) 155-164, doi:10.1016/j.jcat.2011.06.006.

[34] M. Badawi, S. Cristol, J.-F. Paul, E. Payen, DFT study of furan adsorption over stable molybdenum sulfide catalyst under HDO conditions, C. R. Chim. 12 (6) (2009) 754-761, doi:10.1016/j.crci.2008.10.023.

[35] G. Kresse, J. Hafner, Ab initio molecular dynamics for liquid metals, Phys. Rev. B 47 (1) (1993) 558, doi:10.1103/PhysRevB.47.558.

[36] P.E. Blöchl, Projector augmented-wave method, Phys. Rev. B 50 (24) (1994) 17953, doi:10.1103/PhysRevB.50.17953.

[37] G. Kresse, D. Joubert, From ultrasoft pseudopotentials to the projector augmented-wave method, Phys. Rev. B 59 (3) (1999) 1758, doi:10.1103/PhysRevB.59.1758.

[38] J.P. Perdew, K. Burke, M. Ernzerhof, Generalized Gradient Approximation Made Simple, Phys. Rev. Lett. 77 (18) (1996) 3865, doi:10.1103/PhysRevLett.77.3865.

[39] S. Grimme, Semiempirical GGA-type density functional constructed with a long-range dispersion correction, J. Comput. Chem. 27 (15) (2006) 1787-1799, doi:10.1002/jcc.20495.

[40] T. Bučko, J. Hafner, S. Lebègue, J.G. Ángyán, Improved description of the structure of molecular and layered crystals: Ab initio DFT calculations with van der Waals corrections, J. Phys. Chem. A 114 (43) (2010) 11814-11824, doi:10.1021/jp106469x.

[41] H. Akram, C. Mateos-Pedrero, E. Gallegos-Suárez, A. Guerrero-Ruíz, T. Chafik, I. Rodríguez-Ramos, Effect of electrolytes nature and concentration on the morphology and structure of MoS_2 nanomaterials prepared using one-pot solvothermal method, Appl. Surf. Sci. 307 (2014) 319-326, doi:10.1016/j.apsusc.2014.04.034.

[42] D. Wang, B. Su, Y. Jiang, L. Li, B.K. Ng, Z. Wu, F. Liu, Polytype 1T/2H MoS_2 heterostructures for efficient photoelectrocatalytic hydrogen evolution, Chem. Eng. J. 330 (2017) 102-108, doi:10.1016/j.cej.2017.07.126.

[43] J. Xie, J. Zhang, S. Li, F. Grote, X. Zhang, H. Zhang, R. Wang, Y. Lie, B. Pan, Y. Xie, Controllable disorder engineering in oxygen-incorporated MoS_2 ultrathin nanosheets for efficient hydrogen evolution, J. Am. Chem. Soc. 135 (47) (2013) 17881-17888, doi:10.1021/ja408329q.

[44] X. Zhang, Z. Lai, C. Tan, H. Zhang, Solution-processed two-dimensional MoS_2 nanosheets: Preparation, hybridization, and applications, Angew. Chem. Int. Edit. 55 (31) (2016) 8816-8836, doi:10.1002/anie.201509933.

[45] K.D. Rasamani, F. Alimohammadi, Y. Sun, Interlayer-expanded MoS_2, Mater. Today 20 (2) (2017) 83-91, doi:10.1016/j.mattod.2016.10.004.

[46] M. Yi, C. Zhang, The synthesis of two-dimensional MoS_2 nanosheets with enhanced tribological properties as oil additives, RSC Adv. 17 (8) (2018) 9564-9573, doi:10.1039/c7ra12897e.

[47] X. Zhang, Z. Du, X. Luo, A. Sun, Z. Wu, D. Wang, Template-free fabrication of hierarchical MoS_2 /MoO_2 nanostructures as efficient catalysts for hydrogen production, Appl. Surf. Sci. 433(2018) 723-729, doi:10.1016/j.apsusc.2017.10.105.

[48] Y. Xia, Y. He, C. Chen, Y. Wu, J. Chen, MoS_2 nanosheets modified SiO_2 to enhance the anticorrosive and mechanical performance of epoxy coating, Prog. Org. Coat. 132 (2019) 316-327, doi:10.1016/j.porgcoat.2019.04.002.

[49] G. Liu, J. Cui, R. Luo, Y. Liu, X. Huang, N. Wu, X. Jin, H. Chen, S. Tang, J-K. Kim, X. Liu, 2D MoS_2 grown on biomass-based hollow carbon fibers for energy storage, Appl. Surf. Sci. 469 (2019) 854-863, doi: 10.1016/j.apsusc.2018.11.067.

[50] H. Wu, L. Wang, B. Johnson, S. Yang, J. Zhang, G. Dong, Investigation on the lubrication advantages of MoS_2 nanosheets compared with ZDDP using block-on-ring tests, Wear 394-395 (2018) 40-49, doi:10.1016/j.wear.2017.10.003.

[51] O. Tevet, P. Von-Huth, R. Popovitz-Biro, R. Rosentsveig, H.D. Wagner, R. Tenne, Friction mechanism of individual multilayered nanoparticles, P. Natl. Acad. Sci. USA 108 (50) (2011) 19901-19906, doi:10.1073/pnas.1106553108.

[52] K.H. Hu, X.G. Hu, Y.F. Xu, F. Huang, J.S. Liu, The effect of morphology on the tribological properties of MoS_2 in liquid paraffin, Tribol. Lett. 40 (1) (2010) 155-165, doi:10.1007/s11249-010-9651-z.

[53] I. Lahouij, B. Vacher, J.-M. Martin, F. Dassenoy, IF-MoS_2 based lubricants: Influence of size, shape and crystal structure, Wear 296 (1-2) (2012) 558-567, doi:10.1016/j.wear.2012.07.016.

[54] H. Wu, L. Qin, G. Dong, M. Hua, S. Yang, J. Zhang, An investigation on the lubrication mechanism of MoS_2 nano sheet in point contact: the manner of particle entering the contact area, Tribol. Int. 107 (2017) 48-55, doi:10.1016/j.triboint.2016.11.009.

[55] J. Tannous, F. Dassenoy, I. Lahouij, T. Le Mogne, B. Vacher, A. Bruhás, W. Tremel, Understanding the tribochemical mechanisms of IF-MoS_2 nanoparticles under boundary lubrication, Tribol. Lett. 41 (1) (2011) 55-64, doi:10.1007/s11249-010-9678-1.

[56] N. Rajendhran, S. Palanisamy, P. Periyasamy, R. Venkatachalam, Enhancing of the tribological characteristics of the lubricant oils using Ni-promoted MoS_2 nanosheets as nano-additives, Tribol. Int. 118 (2018) 314–328, doi:10.1016/j.triboint.2017.10.001.

[57] L. Liu, Z. Huang, P. Huang, Fabrication of coral-like MoS_2 and its application in improving the tribological performance of liquid paraffin, Tribol. Int. 104 (2016) 303–308, doi:10.1016/j.triboint.2016.09.013.

[58] P. Rabaso, F. Dassenoy, F. Ville, M. Diaby, B. Vacher, T. Le Mogne, M. Belin, J. Cavoret, An investigation on the reduced ability of IF-MoS_2 nanoparticles to reduce friction and wear in the presence of dispersants, Tribol. Lett. 55 (2014) 503 516, doi:10.1007/s11249-014-0381-5.